ELSEVIER

Journal of Nuclear Materials 312 (2003) 249–256

journal of nuclear materials

www.elsevier.com/locate/jnucmat

Solubility studies, thermodynamics and electrical conductivity in the $Th_{1-x}Sr_xO_2$ system

R. Subasri [a], C. Mallika [a], T. Mathews [a], V.S. Sastry [b], O.M. Sreedharan [a,*]

[a] *Thermodynamics and Kinetics Division, Materials Characterisation Group, Indira Gandhi Centre for Atomic Research, Kalpakkam, Tamil Nadu 603 102, India*

[b] *Material Science Division, Indira Gandhi Centre for Atomic Research, Kalpakkam, Tamil Nadu 603 102, India*

Received 7 March 2002; accepted 22 November 2002

Abstract

A polymeric gel combustion method was employed for the lower temperature synthesis of 1, 2, 3, 5, 7.5, 10 and 15 mol.% SrO doped ThO_2 solid solutions. After final sintering of these samples at 1573 K in Ar, the solubility limit was found to be 1 mol.%, giving rise to a composition-independent value of (559.84 ± 0.02) pm (at 300 K) for the CaF_2-type unit cell. AC impedance measurements carried out on discs of 1, 2, 3 and 5 mol.% SrO in ThO_2 discs in flowing Ar, yielded values of 116, 115, 128 and 96 kJ/mol, respectively as the activation energies for the bulk ionic conductivity. The thermodynamic activities of SrO in the 1, 2 and 3 mol.% solid solutions were measured using $[SrO]_{ThO_2}$,SrF_2,O_2,Pt as the test electrodes and $SrZrO_3$,ZrO_2,SrF_2,O_2,Pt as the reference with sintered SrF_2 as the electrolyte over the range of approximately 650–800 K. The activity values differed marginally from each other, but were indicative of the combined (and not free) state of SrO. Hence, only a limiting value of a_{SrO} for the just saturated (mole fraction of SrO = 0.01) thoria solid solution could be derived as $\log a_{SrO} = 0.36 - 4602/T$ (K).

1. Introduction

Thorium is expected to play an important role in the third stage of the Indian Nuclear Energy Program. The physico-chemical properties of dilute solutions of alkaline-earth (AE) oxides in the thoria matrix are of considerable relevance to Advanced Heavy Water Reactors, since Ba and Sr are among the predominant fission products [1]. The electrical properties of the fluorite structured solid solutions of AE and rare earth oxides in ThO_2 and ZrO_2 reported in the literature prior to 1969 were reviewed by Etsell and Flengas in the light of their applications as solid electrolytes [2]. Since the solubility of BaO in ThO_2 was reported to be rather restricted to less than 1 mol.% as compared to 3–5 mol.% of SrO, the present studies were undertaken on the latter to identify systematic trends if any, in the properties with dopant concentrations. It should be mentioned that there is a considerable scatter in the crystallographic lattice parameters reported in the literature based on which the solubility limits were predicted [3,4]. Hence, there is a case for redetermining the lattice parameters to assess the solubility limit. Moreover, there are no reliable reports available in the literature on the conductivity of ThO_2–SrO solid solutions. In addition, the high temperature thermodynamic activity of SrO in these solid solutions though important, has not hitherto been reported even by solid electrolyte emf measurements. The difficulties in identifying a suitable oxide electrolyte have precluded such measurements by the emf technique. The present investigation is aimed at addressing the above-mentioned issues by devising suitable experimental strategies.

* Corresponding author. Address: Department of Atomic Energy, Metallurgy and Materials Group, Indira Gandhi Centre for Atomic Research, Kalpakkam, Tamil Nadu 603 102, India. Tel.: +91-4114 480 116; fax: +91-4114 480 381/40301.

E-mail address: oms@igcar.ernet.in (O.M. Sreedharan).

0022-3115/03/$ - see front matter
PII: S0022-3115(02)01648-3

2. Experimental

2.1. Materials

Reagent grade $Sr(NO_3)_2$ (s.d. Fine Chem., India) and $Th(NO_3)_4 \cdot 6H_2O$ (Fisons, USA) with total metallic impurities less than 0.02% were used as the starting materials for the solid solutions. In addition, $SrCO_3$ (Loba-Chemie, India) and ZrO_2 (Johnson Matthey, UK) of purity better than 99.99% were used for the solid-state synthesis of $SrZrO_3$. Polycrystalline SrF_2 (Aldrich, USA) of purity 99.99% was used for making the electrolyte discs. Other chemicals such as nitric acid, citric acid and ethylene glycol were of reagent grade.

2.2. Synthesis

The solid solutions of compositions 1, 2, 3, 5, 7.5, 10 and 15 mol.% SrO in ThO_2 were prepared as per the procedure depicted as a flow chart in Fig. 1. The final sintering was carried out at a temperature of 1573 K for 24 h under Ar (purity better than 99.99% with respect to free oxygen as impurity).

The interoxide $SrZrO_3$ was synthesized through the solid-state reaction route by intimately grinding a mixture of ZrO_2 and $SrCO_3$ in the mole ratio 1.1:1 which was heat-treated at 1523 K for 72 h with intermittent grinding and compacting. Since $SrZrO_3$ coexists with ZrO_2 as per the phase diagram available in the literature [5], an excess of ZrO_2 (10 mol.%) was taken to ensure completion of the reaction of $SrCO_3$ with ZrO_2.

Some of the routine phase identifications were carried out by Rigaku Model, powder X-ray diffractometer (XRD) with Cu target and graphite monochromator, within its 5 mass% threshold limits of detection of impurity phases. However, for accurate lattice parameter calculations, a STOE precision X-ray powder diffractometer using Bragg–Brentano parafocussing geometry was made use of. The ambient temperature during XRD measurements was around 300 K. The diffractometer had a diffracted beam monochromator with an overall instrumental resolution of $2\theta = 0.14°$ at the 28.442° Si(1 1 1) line. The sub-micron powders of ThO_2–SrO solid solutions resulting from the soft chemistry (polymeric gel combustion, PGC) route had to be subjected to the particle size analysis by measuring the line broadening. The crystallite size was calculated using the Debye–Scherrer formula

$$t = 0.97\lambda/\beta\cos\theta_B, \quad (1)$$

where t indicates the particle size in nanometer and λ the incident X-ray wavelength. β is a radian measure of full width at half maximum (FWHM) and $2\theta_B$ is the angle subtended at maximum intensity. FWHM was calculated after correcting for the contribution by the X-ray machine. The background subtraction, $K\alpha_2$ stripping, peak search, indexing, lattice parameter calculation and crystallite size analyses were accomplished using WinXPow suite of powder diffraction data analysis package. The duration of the heat treatment at 1573 K was optimized to be 24 h to minimize the surface energy contributions to thermodynamic properties. After sintering, the pellets were stored in a desiccator except while in use. This precaution was taken to avoid disintegration of pellets on interaction with humid (70% RH) environment. The pellets with more than 7.5 mol.% SrO were found to disintegrate into fine powder on exposure to humid environment if not stored in vacuum or under a dried inert gas.

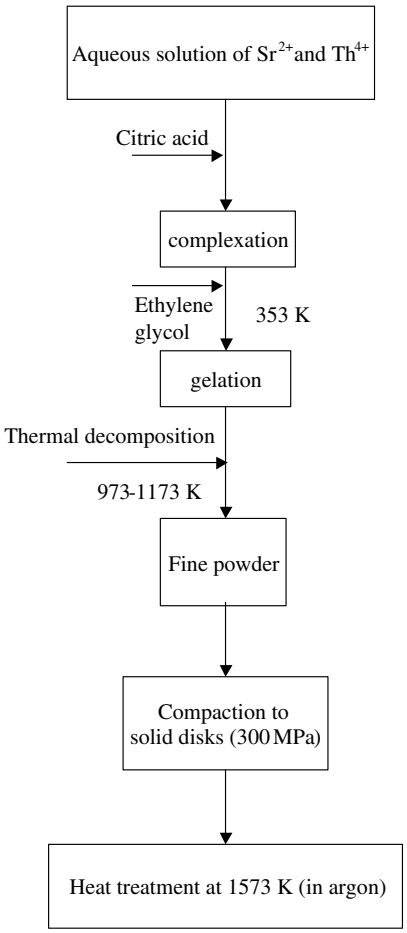

Fig. 1. Flow sheet for the synthesis of ThO_2 doped with SrO.

The electrolyte discs were made by compacting polycrystalline SrF_2 into those of 15 mm diameter and 3–4 mm thickness at a pressure of 300 MPa. These pellets were gradually heated to 1523 K and soaked for 5 h under the cover of Ar gas, followed by slow cooling to 1473 K where it was isothermally maintained for 12 h

and subsequently cooled to the ambient. This heating schedule was planned to avoid any porosity due to vapourization. The density of the pellets was measured with dibutyl phthalate as the pycnometric fluid by employing a density kit (M/s. Precisa Instruments, Switzerland). The average density of four such discs was found to be 3.918 Mg/m^3 (>93% theoretical).

2.3. Methods

Electrical conductivity measurements were carried out on ThO_2 doped with 1, 2, 3 and 5 mol.% SrO over a frequency range of 1 MHz to 50 Hz and an AC voltage of 10 mV using a frequency response analyzer (Eco-Chemie, The Netherlands). Platinum ink (Engelhard, USA) was applied over the parallel surfaces of the sintered discs and baked in air at 1023 K for 3 h to ensure complete elimination of organics from the suspension thereby forming a porous network of adherent platinum. The temperature range employed was 620–900 K. The atmosphere during the measurements was maintained to be dry Ar gas with a $p(O_2)$ of the order of 10^{-5} bar to ensure the measurements to be within the electrolytic domain ($t(O^{2-}) > 0.99$) of ThO_2–SrO. Since the measurements are prone to AC pick-up, the impedance cell was enveloped with an Inconel foil and was suitably earthed.

An open-cell stacked-pellet assembly as described elsewhere [6], was employed for the emf measurements. Pure O_2 at 1 bar pressure was used as the cover gas after passing through suitable drying columns. All emf measurements were made over the temperature range of about 650–800 K. The temperature range was rather restricted by many factors. For instance, the upper limit was dictated by the sintering of finely divided Pt (which otherwise functions as a catalyst for electron transfer) and also by the probable vapourization of SrF_2. The lower temperature was restricted by the kinetics of attainment of equilibrium. All temperature measurements were made using a pre-calibrated Type-S (Pt/Pt–10% Rh) thermocouple whose hot junction was located in the proximity of the galvanic cell, which in turn was placed in the uniform temperature zone to minimize thermoelectric contributions. All other experimental precautions were the same as described elsewhere [6,7]. The test electrode pellets were made by compaction as described earlier from an intimate mixture of the solid solutions with an equal mass of SrF_2. In the case of reference electrode, an additional quantity of ZrO_2 was added to the pre-equilibrated (1:0.1 mole ratio) mixture of $SrZrO_3$ and ZrO_2 in order to make it roughly equimolar and then mixed with SrF_2 before compacting into an electrode disc.

The following galvanic cell configurations were assembled and the emf of the cells was measured as a function of temperature.

$$(-)\mathrm{Pt}, O_2(1.013\ \mathrm{bar}), ZrO_2, SrZrO_3, SrF_2|SrF_2|\ ThO_2\text{–}1\ \mathrm{mol.\%}\ SrO, SrF_2, O_2(1.013\ \mathrm{bar}), \mathrm{Pt}(+) \quad (\mathrm{I})$$

$$(-)\mathrm{Pt}, O_2(1.013\ \mathrm{bar}), ThO_2\text{–}2\ \mathrm{mol.\%}\ SrO, SrF_2|\ SrF_2|ZrO_2, SrZrO_3, SrF_2, O_2(1.013\ \mathrm{bar}), \mathrm{Pt}(+) \quad (\mathrm{II})$$

$$(-)\mathrm{Pt}, O_2(1.013\ \mathrm{bar}), ThO_2\text{–}3\ \mathrm{mol.\%}\ SrO, SrF_2|SrF_2|\ ZrO_2, SrZrO_3, SrF_2, O_2(1.013\ \mathrm{bar}), \mathrm{Pt}(+) \quad (\mathrm{III})$$

$$(-)\mathrm{Pt}, O_2(1.013\ \mathrm{bar}), ThO_2\text{–}3\ \mathrm{mol.\%}\ SrO, SrF_2|SrF_2|\ ThO_2\text{–}2\ \mathrm{mol.\%}\ SrO, SrF_2, O_2(1.013\ \mathrm{bar}), \mathrm{Pt}(+) \quad (\mathrm{IV})$$

$$(-)\mathrm{Pt}, O_2(1.013\ \mathrm{bar}), ThO_2\text{–}15\ \mathrm{mol.\%}\ SrO, SrF_2|SrF_2|\ ZrO_2, SrZrO_3, SrF_2, O_2(1.013\ \mathrm{bar}), \mathrm{Pt}(+) \quad (\mathrm{V})$$

Galvanic cell IV was used for checking the reversibility as well as the consistency between the emf data from the galvanic cells II and III.

3. Results and discussion

3.1. Solubility

The lattice parameters of the seven solid solutions as well as that of pure thoria were computed by a non-linear regression analysis of the XRD results. The cubic cell parameter, a of these fluorite-structured matrices is listed in Table 1 and plotted against mole fraction in Fig. 2. Prior to comparing the solubility limit of SrO in ThO_2 and the corresponding lattice parameter of the solid solutions, the reliability of the a value reported in Table 1 for pure thoria has to be checked. The accepted lattice parameter for pure thoria reported in the literature is (559.72 ± 0.02) pm [8] based on about 20 original data and it compares well with the presently reported value of (559.76 ± 0.02) pm (Table 1). In another compilation [9] on the physical properties of thoria, a value of (559.75 ± 0.03) pm is recommended for a at 298 K. Taking into account the assessed value of 5×10^{-5} for

Table 1
Lattice parameters of SrO doped thoria

Mol.% SrO	a (pm)	Figure of merit
0	559.76 ± 0.02	133.6
1	559.83 ± 0.02	102.8
2	559.86 ± 0.02	149.1
3	559.82 ± 0.03	100.6
5	559.87 ± 0.02	169.4
7.5	559.83 ± 0.02	100.8
10	559.86 ± 0.01	156.8
15	559.82 ± 0.02	97.5

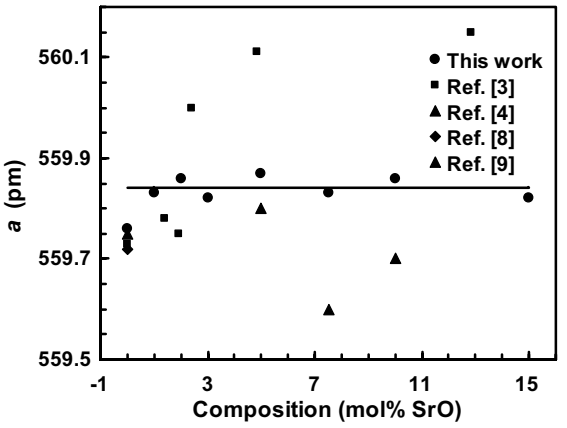

Fig. 2. Lattice parameter against mol.% of SrO in ThO_2–SrO.

the thermal expansion coefficient, $\Delta L/L$ of thoria at 298 K, the difference between the above three values in the lattice parameter should be considered as negligible.

Within the limits of experimental scatter (±0.01 to 0.03 pm), the results presented in Table 1 and Fig. 2 revealed the invariance of a with composition giving rise to a mean value of 559.84 pm for the fluorite structured thoria saturated with about 1 mol.% of SrO. No attempt was made to synthesize solid solutions between 0% and 1% for identifying the exact composition of saturation solubility owing to analytical limitations. A comparison has also been made with the results reported by Möbius et al. [3] (up to 12.82 mol.% only instead of up to 49.79 mol.% SrO, reported by them) and Tyagi et al. [4] (above 559.5 pm only instead of up to 559.2 pm reported by them for 1 mol.% SrO) in Fig. 2. These authors reported solubility limits of 4 and 5 mol.% respectively for SrO in thoria with the mean values of (560.13 ± 0.02) pm and (559.7 ± 0.1) pm for the lattice parameter of thoria saturated with strontia. The difference in the values of a between the three sets could be attributed mainly to the difference in the sintering temperatures and perhaps to the starting materials and the gaseous environment during sintering. In the present work, the solid solutions were obtained by sintering the sub-micron powders (resulting from the PGC method) at 1573 K for 24 h in Ar. In contrast, Tyagi et al. heated the mechanically mixed powders of $SrCO_3$ and ThO_2 at 1923 K for 4 h in flowing N_2–8% H_2 mixture, while Möbius et al. had heated the oxide mixtures at 2073 K for 0.3 h in air. It appears that higher temperatures of sintering resorted to, for solid solution formation from mechanically mixed powders might be resulting in supersaturation of thoria lattice with the solute, SrO. However, upon subsequent cooling, kinetic factors could have played a role in restricting ex-solution of the excess solute from reaching the equilibrium limits. Incidentally, the value of (560.13 ± 0.02) pm for the 4 mol.% solid solution by Möbius et al. was arrived at from those for the five solid solutions ranging from 4.84 to 49.79 mol.% SrO (excluding 8.63 mol.% with $a = 560.23$ pm). The data reported by Tyagi et al. [4] indicate a value of (559.7 ± 0.1) pm for a for the 5 mol.% solid solution. The rather lower value of a for the saturated solid solution is also reflected in that of 559.3 pm reported by them for pure ThO_2 in contrast to the assessed values cited earlier.

The sintered discs of compositions 7.5, 10 and 15 mol.% of SrO disintegrated into powder on exposure to laboratory ambient (70% RH) at 300 K and the rate of disintegration increased with the SrO content. The 10 and 15 mol.% solutions were nearly fine powders, whose examination by XRD on the expanded scale revealed the presence of $Sr(OH)_2 \cdot H_2O$. The absence of disintegration of pellets corresponding to 1–3 mol.% SrO on exposure to the ambient environment could not be taken as an evidence for solid solution formation, but might nevertheless preclude free SrO.

3.2. Electrical conductivity

A typical plot of the imaginary component ($-Z''$) of the impedance of ThO_2–5 mol.% SrO disc at 773 K against the real component (Z) is shown in Fig. 3. It is evident from this figure that the data points fit into a single arc, characteristic of bulk conduction. Further, the samples under investigation were highly resistant materials, which obviate the need to subtract the contribution of the lead resistance from the measured one. By collecting the earlier points of intersection of such arcs with the x-axis, a plot of $\log \sigma T$ against the reciprocal temperature was constructed for each sample and the least-squares regression lines for the four compositions are shown in Fig. 4. The overall temperature range

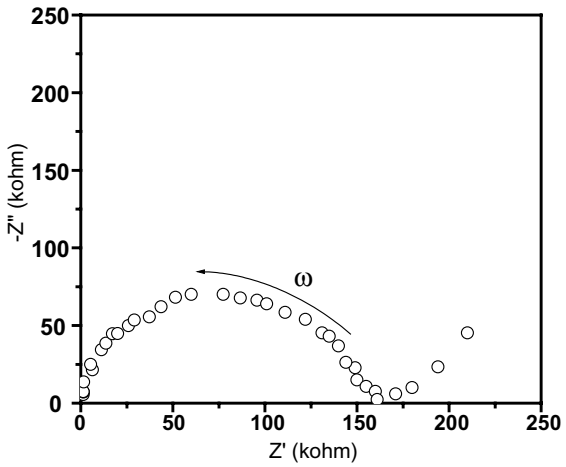

Fig. 3. Plot of $-Z''$ against Z for 5 mol.% SrO in ThO_2 at 773 K.

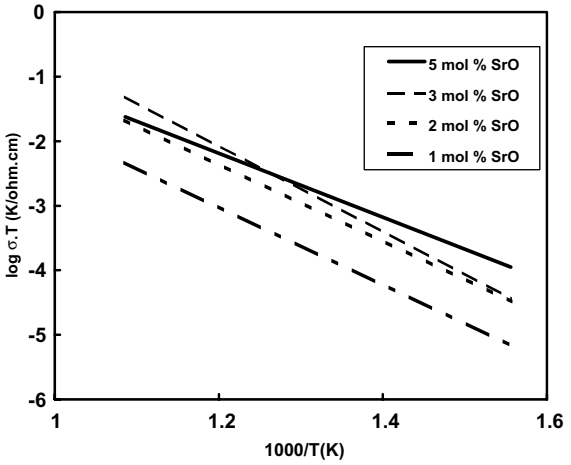

Fig. 4. Inverse temperature dependence of the electrical conductivity of ThO_2–SrO solid solutions.

covered was 600–900 K for these samples. From these expressions, the activation energies were calculated and the conductivity values interpolated at a mean temperature of approximately 800 K are listed in Table 2. The extrapolated values at 1273 K are compared with those reported in the literature [10,11]. The values of isothermal conductivity at 800 K (Table 2) reveal only a moderate increase with dopant concentration for the first three compositions while that for the 5 mol.% sample is slightly lower than the 3 mol.%. The effect of SrO as dopant on the conductivity is found to be not quite significant. In the light of the fact that the saturation solubility of SrO is about 1% or less, the contribution of doubly ionized oxide ion vacancies to the ionic conductivity should be more or less constant in the biphasic regime, which commences right from 1%. Further, the contribution due to hole conductivity should not be significant since the measurements were made in an environment of inert gas (with $p(O_2) < 10^{-5}$ bar). Therefore, these conductivity results should be considered as almost those for bulk ionic conductivity registering only a marginal increase in the biphasic regime.

The limited solubility of SrO could be understood by computing the critical dopant radius (suggested by Kim [12]) using the expression:

$$d_{\mathrm{Th}}\ (\mathrm{nm}) = 0.5596 + (0.0212\,\Delta r_k + 0.00011\,\Delta z_k)m_k, \quad (2)$$

where d_{Th} is the lattice constant of the fluorite oxide solid solution at room temperature, Δr_k is the difference in ionic radius ($r_k - r_h$) of the kth dopant and the host cation in eight-fold coordination, Δz_k is the valency difference ($z_k - z_h$) and m_k is the mole percent of the kth dopant in the form of MO_x. The critical ionic radius is calculated by setting the slope in Eq. (2) to zero. Accordingly, the critical ionic radius derived for the divalent dopant for Th^{4+} in fluorite structured ThO_2 is 0.1294 nm (129.4 pm). The lower the difference between the true ionic radii and the critical ionic radius, the greater the enhancement in conductivity. In other words, dopants which cause very little expansion or contraction in the host lattice will lead to enhancement in conductivity. Obviously, this is not the case since the ionic radius of 140 pm for Sr^{2+} is much greater than the critical value, perhaps accounting for its limited solubility in the host matrix.

From the foregoing considerations, one should expect a greater conductivity (also ionic) in the case of Ca^{2+} and lower values for Ba^{2+} as dopants for similar concentrations. Since such results are not available in the published literature, only a qualitative comparison is made in Table 2 for 5 mol.% Ca^{2+} and 15 mol.% Ba^{2+} solid solutions (or mixtures?), that too in air atmosphere.

3.3. Thermodynamic activity

The emf results on cells I–IV are plotted as a function of temperature in Fig. 5. The least-squares expressions corresponding to this plot are listed in Table 3 along with the respective temperature ranges of emf measurements. The reference electrodes used for the cells I–III were identical, viz: $Pt,O_2(1.013\ bar),ZrO_2,SrZrO_3,SrF_2$. However, the configuration of cell IV was designed to eliminate the use of $SrZrO_3$ bearing reference electrode

Table 2
Electrical conductivities of CaO, SrO and BaO doped ThO_2

Composition	E_a (kJ/mol)	$\sigma_{800\ K}$ ($ohm^{-1}\,cm^{-1}$)	$\sigma_{1273\ K}$ ($ohm^{-1}\,cm^{-1}$)	Ref.
$(SrO)_{0.01}(ThO_2)_{0.99}$	116	5.9×10^{-7}	2.4×10^{-4}	This work
$(SrO)_{0.02}(ThO_2)_{0.98}$	115	2.8×10^{-6}	1.1×10^{-3}	This work
$(SrO)_{0.03}(ThO_2)_{0.97}$	128	4.9×10^{-6}	3.8×10^{-3}	This work
$(SrO)_{0.05}(ThO_2)_{0.95}$	96	4.5×10^{-6}	6.1×10^{-4}	This work
$(CaO)_{0.05}(ThO_2)_{0.95}$	106[a]	–	7.5×10^{-4}	[10]
$(SrO)_{0.15}(ThO_2)_{0.85}$	77[a]	–	1.4×10^{-3}	[11]
$(BaO)_{0.15}(ThO_2)_{0.85}$	72[a]	–	4.4×10^{-3}	[11]

[a] Measured in air.

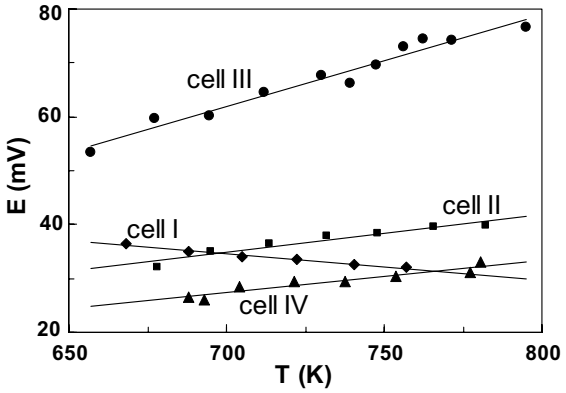

Fig. 5. Temperature dependence of the emf of cells I–IV.

by employing the test electrode configurations of cells III and II as those of anode and cathode (of cell IV), respectively. The purpose of assembling such a galvanic cell was to check the internal consistency among the emf results from cells II–IV. For instance, if the cells II and IV were connected in series, the resultant emf (which is the algebraic sum of the emf values of the two cells at the corresponding temperature) should agree with those for cell III within the limits of quoted precision. Thus, at 650 and 750 K, the algebraic sum of the values of emf for cells IV and II were 55.7 ± 1.6 $(24.3 + 31.4)$ and 68.8 ± 1.6 $(30.4 + 38.4)$ mV in good agreement with those of 53.4 ± 1.5 and 70.4 ± 1.5 mV respectively by interpolating from the least-squares expressions for the three cells from Table 3. This upholds the internal consistency among the emf results from the different cells. The emf results on cell V are not included in either Fig. 5 or Table 3 because a value of 373 mV lasting for several hours with a drift of less than 0.2 mV/h could be recorded only at one temperature namely 795 K. Below this temperature, the build-up of emf was very slow without reaching a steady value and at temperatures significantly beyond 800 K, there was a rapid drop in the emf as was observed in the case of other cells.

The half-cell reactions and the overall virtual cell reaction corresponding to two faraday of electricity for cell I may be represented as

$$[\mathrm{SrO}]_{\mathrm{SrZrO_3,ZrO_2}} + 2\mathrm{F}^{-1} \rightarrow \mathrm{SrF_2} + 1/2\mathrm{O_2} + 2\mathrm{e}^{-1} \quad (3a)$$

$$\mathrm{SrF_2} + 1/2\mathrm{O_2} + 2\mathrm{e}^{-1} \rightarrow [1\ \text{mol.\%}\ \mathrm{SrO}]_{\mathrm{ThO_2}} + 2\mathrm{F}^{-1} \quad (3b)$$

$$[\mathrm{SrO}]_{\mathrm{SrZrO_3,ZrO_2}} \rightarrow [1\ \text{mol.\%}\ \mathrm{SrO}]_{\mathrm{ThO_2}} \quad (3)$$

For this virtual cell reaction, the Gibbs energy change, $\Delta_r G^0$ was calculated using the Nernst equation:

$$\Delta_r G^0 = -2FE_1, \quad (4)$$

which corresponds to

$$\Delta_r G^0(\mathrm{I}) = \Delta\overline{\mathrm{G}}([1\ \text{mol.\%}\ \mathrm{SrO}]_{\mathrm{ThO_2}}) - \Delta\overline{\mathrm{G}}([\mathrm{SrO}]_{\mathrm{SrZrO_3,ZrO_2}}). \quad (5)$$

For computing the partial molar Gibbs energy of SrO, $\Delta\overline{G}_{\mathrm{SrO}}$ in the coexisting $SrZrO_3/ZrO_2$ mixture, use is made of the solid–solid reaction

$$\mathrm{SrO} + \mathrm{ZrO_2} \rightarrow \mathrm{SrZrO_3} \quad (6)$$

The standard Gibbs energy change for the reaction (6) is identical with the standard Gibbs energy of formation, $\Delta_f G^0_{\mathrm{ox}}$ of $SrZrO_3$ from the constituent binary oxides. Thus,

$$\Delta_r G^0\ (6) = \Delta_f G^0_{\mathrm{ox}}(\mathrm{SrZrO_3}) = RT \ln a_{\mathrm{SrO}}, \quad (7)$$

((i.e) $\Delta\overline{G}_{\mathrm{SrO}}$ in $SrZrO_3/ZrO_2$).

Owing to the higher activity of SrO in the test electrodes of cells II and III, the overall virtual cell reactions would correspond to the reversal in direction to that of Eq. (3) namely

$$[2\ \text{mol.\%}\ \mathrm{SrO}]_{\mathrm{ThO_2}} \rightarrow [\mathrm{SrO}]_{\mathrm{SrZrO_3,ZrO_2}} \quad (8)$$

and

$$[3\ \text{mol.\%}\ \mathrm{SrO}]_{\mathrm{ThO_2}} \rightarrow [\mathrm{SrO}]_{\mathrm{SrZrO_3,ZrO_2}} \quad (9)$$

Substituting the emf results on cells I–III (Table 3) in the Nernst equation (4), the numerical expressions for $\Delta_r G^0$ were calculated.

$$\Delta_r G^0(\mathrm{I}) \pm 0.1\ (\mathrm{kJ/mol}) = -13.2 + 0.0093T\ (\mathrm{K}), \quad (10)$$

Table 3
Coefficients of linear fits of the emf data for cells I–IV

Cell	E (mV) $= A + BT$ (K)		Precision (mV)	T range (K)	E (mV) at 750 K
	A (mV)	B (mV/K)			
I	68.4	−0.0482	±0.3	668–757	32.3
II	−14.1	0.0700	±0.8	678–782	38.4
III	−57.1	0.1700	±1.5	657–795	70.4
IV	−14.8	0.0602	±0.8	688–780	30.4

$$\Delta_r G^0(\mathrm{II}) \pm 0.2\ (\mathrm{kJ/mol}) = 2.7 - 0.0135T\ (\mathrm{K}), \quad (11)$$

$$\Delta_r G^0(\mathrm{III}) \pm 0.3\ (\mathrm{kJ/mol}) = 11.0 - 0.0328T\ (\mathrm{K}). \quad (12)$$

The $\Delta_r G^0$ for cell IV was likewise derived to be

$$\Delta_r G^0(\mathrm{IV}) \pm 0.2\ (\mathrm{kJ/mol}) = 2.9 - 0.0116T\ (\mathrm{K}) \quad (13)$$

by combining E_{IV} (Table 3) with Eq. (4). Eq. (13) could be used for comparing the consistency between the expressions (11) and (12).

To facilitate the calculation of $\Delta\overline{G}_{\mathrm{SrO}}$ in the 1, 2 and 3 mol.% SrO solid solutions, an expression for $\Delta_f G^0_{\mathrm{ox}}$ ($\Delta\overline{G}_{\mathrm{SrO}}$ in $SrZrO_3/ZrO_2$) valid over the range 600–800 K was required. For this purpose, Gibbs energy data compiled by Knacke et al. [13] for the relevant oxides were made use of to derive the following linear fit:

$$\Delta_f G^0_{\mathrm{ox}}(SrZrO_3)\ (\mathrm{kJ/mol}) = -74.9 - 0.0024T\ (\mathrm{K}). \quad (14)$$

The numerical expressions for $\Delta\overline{G}_{\mathrm{SrO}}$ for the three compositions of ThO_2–SrO derived by combining Eqs. (10)–(12) and (14) using the equality $\Delta\overline{G}_{\mathrm{SrO}} = RT\ln a_{\mathrm{SrO}}$ are listed in Table 4. It is seen from this Table that the value of a_{SrO} (as seen for instance that interpolated at 750 K) increases from 0.17×10^{-5} to 4.1×10^{-5} for 1–3 mol.% SrO. This observation is not consistent with the expectation of constancy of isothermal activity over the biphasic region (vide XRD results from Table 1) commencing from about 1 mol.% SrO. Even if SrO existing in excess of 1 mol.% precipitates out from the host matrix as a stable ternary oxide phase say $SrThO_3$, it should still give rise to an isothermal activity of SrO independent of composition.

However, Ali et al. [14] estimated the $\Delta_f G^0_{\mathrm{ox}}$ of $SrThO_3$ from high temperature (1670–2040 K) Knudsen effusion forward collection technique on $SrThO_3$/W/Sr_2WO_5/ThO_2/Sr(g) equilibrium. This estimate shows $SrThO_3$ to be only marginally stable, (-2.7 ± 4.0) kJ/mol if extrapolated down to 750 K, and its formation need not be considered. Likewise, $Sr(OH)_2$ is also too unstable to account for the lowering of SrO activity as inferred from a temperature of 476 K [13] for the dissociation of $Sr(OH)_2$ (in the galvanic cell atmosphere of O_2 gas dried to a level of 1 vpm (volume part per million) of H_2O vapour). However, the possibility of a carbonate complex formation by SrO in excess of saturation solubility of about 1 mol.% could not be ruled out because of the higher stability of $SrCO_3$ and the ubiquitous nature of CO_2 formed from the carbonaceous impurities present in otherwise dried O_2 cover gas. The CO_2 trapped in the grains could result in the lowering of SrO activity by three orders at 600–700 K corresponding to about 1 vpm of CO_2 in O_2.

When the SrO content is 7.5 mol.% or more, the pellets were observed to disintegrate into powder on exposure to humid ambient atmosphere (cf: Section 2.2). The XRD examination on the expanded scale revealed the product to contain $Sr(OH)_2 \cdot H_2O$. The presence of free SrO in the pellets bearing more than 7.5 mol.% of the same is further corroborated by the only emf value recorded for cell V as mentioned earlier. Thus, the value of 373 mV recorded for cell V at 795 K is close to a theoretical value of 398 mV corresponding to the emf of the following hypothetical cell

$$(-)\mathrm{Pt}, O_2(1.013\ \mathrm{bar}), \mathrm{SrO}, SrF_2|SrF_2|ZrO_2, SrZrO_3, SrF_2, O_2(1.013\ \mathrm{bar}), \mathrm{Pt}(+) \quad (\mathrm{VI})$$

This again helps to confirm qualitatively the presence of free SrO in the 15 mol.% sample.

From the foregoing discussion, it is inferred that nearly unit activity of SrO could be identified only for that sample with 15 mol.% SrO, even though one would expect this behaviour even for the sample with 1 mol.% SrO if the results were to be consistent with crystallographic observations. The internally consistent set of emf data among cells I–III amounts to a dissociatable form of SrO in the combined (and not free) state in 1, 2 and 3 mol.% compositions. Hence, only the following activity expression for ThO_2–1 mol.% SrO could be taken as conveying the limiting value of SrO activity in the saturated single phase of thoria.

$$\log a_{\mathrm{SrO}} = 0.36 - 4602/T\ (\mathrm{K}). \quad (15)$$

Making use of the Raoult's law standard state,

$$a_{\mathrm{SrO}} = X_{\mathrm{SrO}}\gamma_{\mathrm{SrO}}, \quad (16)$$

where γ_{SrO} is the activity coefficient. For a composition of 1 mol.% SrO, $\log\gamma_{\mathrm{SrO}}$ could be derived to be

$$\log\gamma_{\mathrm{SrO}} = 2.36 - 4602/T\ (\mathrm{K}). \quad (17)$$

The negative deviation from ideality for the limiting activity coefficient of SrO in ThO_2 just saturated with 1 mol.% solute is indicative of the tendency for compound

Table 4
Comparison of $\Delta\overline{G}_{\mathrm{SrO}}$ in ThO_2–X SrO system ($X_{\mathrm{SrO}} = 0.01$, 0.02 or 0.03)

X_{SrO}	$\Delta\overline{G}_{\mathrm{SrO}}$ ($\mathrm{kJ\,mol^{-1}}$) $= A + BT$ (K)	$\Delta\overline{G}_{\mathrm{SrO}}$ ($\mathrm{kJ\,mol^{-1}}$) at 750 K	$a_{\mathrm{SrO}} \times 10^5$
0.01	$-88.1 + 0.0069T$	−82.9	0.17
0.02	$-77.6 + 0.0111T$	−69.3	1.5
0.03	$-85.9 + 0.0304T$	−63.1	4.1

formation. This indeed is the case as seen from the existence of marginally stable $SrThO_3$ reported in the literature [14].

4. Conclusion

The PGC method paved the way for the synthesis of ThO_2–SrO solid solutions at lower temperatures, which did not result in the supersaturation of the single phase. The precise measurement of the fluorite cubic cell parameter a at ambient temperature for the compositions 1, 2, 3, 5, 7.5, 10 and 15 mol.% SrO indicated the attainment of saturation solubility in all the solutions. A constant value of (559.84 ± 0.02) pm was determined for a of ThO_2 saturated with about 1 mol.% SrO. The reliability of this value is corroborated with the agreement of (559.76 ± 0.02) pm at 300 K measured for a of pure thoria with the value of (559.75 ± 0.03) pm at 298 K assessed in the literature.

The limited solubility of SrO (1 mol.%) in ThO_2 is understandable in the light of critical ionic radius considerations. The AC impedance measurements yielded nearly constant values of activation energy for the 1–3 mol.% SrO compositions which again reflect the limited SrO solubility consequent to the limited formation of the conducting species (doubly ionized oxide ion vacancies).

The fluoride electrolyte emf measurements under O_2 at 1 bar facilitated the determination of limiting activity of SrO near its saturation limit in the thoria matrix.

Acknowledgements

The authors are grateful to Dr Baldev Raj, Director, MCRG and Dr V.S. Raghunathan, Associate Director, MCG of IGCAR, Kalpakkam for their keen interest and constant encouragement throughout the course of this investigation. The authors are also grateful to Dr S.R. Dharwadkar, formerly in the Applied Chemistry Division, BARC, Mumbai for suggesting this work on behalf of the task force on AHWR materials, approved by Dr Anil Kakodkar, Chairman, Atomic Energy Commission, India.

References

[1] P. Rodriguez, C.V. Sundaram, J. Nucl. Mater. 100 (1981) 227.
[2] T.H. Etsell, S.N. Flengas, Chem. Rev. 70 (1970) 340.
[3] H.H. Möbius, H. Witzmann, W. Witte, Z. Chem. 4 (1964) 152.
[4] A.K. Tyagi, M.D. Mathews, R. Ramachandran, J. Nucl. Mater. 294 (2001) 198.
[5] E.M. Levin, H.F. McMurdie, in: M.K. Reser (Ed.), Phase Diagrams for Ceramists, Natl. Bureau Stds., The American Ceramic Society, USA, 1975, p. 128.
[6] O.M. Sreedharan, M.S. Chandrasekharaiah, M.D. Karkhanavala, High Temp. Sci. 9 (1977) 109.
[7] O.M. Sreedharan, E. Athiappan, R. Pankajavalli, J.B. Gnanamoorthy, J. Less-common Met. 68 (1979) 143.
[8] H. Kleykamp, Forschungszentrum Karlsruhe, Institut für Materialforschung, Germany, Private Communication.
[9] I. Cohen, R.M. Berman, J. Nucl. Mater. 18 (1966) 77; J. Belle, R.M. Berman, in: Thorium Dioxide: Properties and Nuclear Applications, Naval Reactors Handbook, Govt. Printing Office, Washington, DC, 1984, p. 69.
[10] Z.S. Volchenkova, S.F. Palguev, in: Electrochemistry of Molten and Solid Electrolytes, Vol. I, Consultants Bureau, New York, 1961, p. 97.
[11] A.D. Neuimin, S.F. Palguev, V.N. Strekalovskii, G.V. Burov, in: M.V. Smirnov (Ed.), Electrochemistry of Molten and Solid Electrolytes, Vol. II, Consultants Bureau, New York, 1964, p. 66.
[12] D.-J. Kim, J. Am. Ceram. Soc. 72 (1989) 1415.
[13] O. Knacke, O. Kubaschewski, K. Hesselmann (Eds.), Thermochemical Properties of Inorganic Substances, 2nd Ed., Springer-Verlag, Germany, 1991.
[14] M. Ali (Basu), R. Mishra, S.R. Bharadwaj, A.S. Kerkar, S.R. Dharwadkar, D. Das, J. Nucl. Mater. 299 (2001) 165.